symmetry

MDPI

Article

Comparative Numerical Analysis for the Error Estimation of the Fluid Flow over an Inclined Axisymmetric Cylinder with a Gyrotactic Microbe

Fuad A. Awwad [1,*], Emad A. A. Ismail [1], Waris Khan [2], Taza Gul [3,4,*] and Abdul Samad Khan [5]

1 Department of Quantitative Analysis, College of Business Administration, King Saud University, P.O. Box 71115, Riyadh 11587, Saudi Arabia; emadali@ksu.edu.sa
2 Department of Mathematics & Statistics, Hazara University, Mansehra 12120, Pakistan; dr.wariskhan@hu.edu.pk
3 Cambridge Graphene Center, University of Cambridge, 9 JJ Thomson Ave, Cambridge CB3 0FA, UK
4 Department of Mathematics, City University of Science and Information Technology, Peshawar 25000, Pakistan
5 Research Center for Computational Science, School of Mathematics and Statistics, Northwestern Polytechnical University, Xi'an 710129, China; abdulsamadkhan17@nwpu.edu.cn
* Correspondence: fawwad@ksu.edu.sa (F.A.A.); tazagul@cusit.edu.pk (T.G.)

Abstract: The numerical investigation of bioconvective nanofluid (NF) flow, which involves gyrotactic microbes and heat and mass transmission analysis above an inclined extending axisymmetric cylinder, is presented in this study. The study aims to investigate the bioconvection flow of nanofluid under the influence of heat sources/sinks. Through proper transformation, all partial differential equations are transformed into a non-linear ODE scheme. A new set of variables is presented in the directive to get the first-order convectional equations and then solved numerically using bvp4c MATLAB, embedded in the function. The proposed model is validated after calculating the error estimation and obtaining the residual error. The influence of various factors on the velocity, energy, concentration, and density of motile microorganisms is examined and studied. The analysis describes and addresses all physical measures of concentration such as Skin Friction (SF), Sherwood number, the density of motile microorganisms, and Nusselt number. To validate the present study, a comparison is conducted with previous studies, and excellent correspondence is found. In addition, the ND-Solve approach is utilized to confirm the bvp4c. The mathematical model is confirmed through error analysis. This study provides the platform for industrial applications such as cooling capacity polymers, heat exchange, and chemical production sectors.

Keywords: computational analysis of fluid flow; gyrotactic microorganism; heat source; thermophoresis; bioconvection Lewis number; stretching axisymmetric cylinder; error estimation

Citation: Awwad, F.A.; Ismail, E.A.A.; Khan, W.; Gul, T.; Khan, A.S. Comparative Numerical Analysis for the Error Estimation of the Fluid Flow over an Inclined Axisymmetric Cylinder with a Gyrotactic Microbe. *Symmetry* **2023**, *15*, 1811. https://doi.org/10.3390/sym15101811

Academic Editors: Dhananjay Yadav, Mukesh Kumar Awasthi and Rishi Asthana

Received: 12 August 2023
Revised: 20 September 2023
Accepted: 21 September 2023
Published: 22 September 2023

1. Introduction

The study of boundary layer flow (BLF) towards an elongating surface was first introduced by Anderson [1] and has become a significant and exciting subject for research investigations because of its wide industrial applications, such as cooling capacity polymers, heat exchange properties such as thermal performance, wire coating-layers, liquid diffusivity, and chemical production sectors. Sakiadis [2,3] examined the BLF over the flat sheet. Further, Crane [4] expanded the study to analyze the changing extending sheet velocity and closed-form analytic solutions obtained for the Navier–Stokes system using two-dimensional flow. These initial assessments have been of extensive significance in the wire performance and elastic fabrication industries. The heat dissemination of the melting liquid has been deliberated [5], where the outcomes have been revealed to be imperative in the development of conserving polymer sheets extracted through a die. Wang [6] amended the fluid dynamic problem outside the stretched tube that is required for the manufacturing environment of cable and fiber pulling. Ishak [7] recently expanded the study of Wang to investigate the melting heat rate over a permeable surface. Keeping the applications of the stretching sheet, many researchers have analyzed the fluid stream and heat transmission over stretching sheets in different conditions. For this goal, nanoparticles were introduced into the base fluid to increase heat transport characteristics such as thickness, thermal efficiency, and diffusivity in the liquid.

Convective heat transfer (CHT) is the most efficient process for heat transmission in liquids. This framework can be improved by varying the movement geometry or boundary constraints, or by improving the thermal characteristics. For instance, the accumulation of nanoparticles with a higher thermal performance in the liquid increases the thermal characteristics of the base fluid.

NF technology has gained significant attention in recent years—particularly in the fields of production, physical science, and materials science. The concept of NF involves adding small quantities of nanoparticles to a base liquid, which enhances its thermal and electrical conductivity, viscosity, and other physical properties [8]. These nanoparticles can be made from a variety of materials, including metals, ceramics, and carbon-based materials. Buongiorno [9] gave the mathematical form of the nanoparticles and determined that a basic mechanism permits us, with prodigious suppleness, to enlighten the thermal features. NFs have been widely used by mathematicians and researchers to study a wide range of practical problems in various fields. In industrial applications [10,11], NFs are used to improve the proficiency of heat transfer systems, which can lead to significant energy savings. In biomedical engineering [12], NFs have been used to develop new diagnostic and therapeutic techniques [13], such as targeted drug delivery systems. In solar thermal applications, NFs are also used to increase the adeptness of solar collectors [14–17] and increase the amount of energy that can be generated from solar power. Numerous studies appear to demonstrate that the emergence of motile microorganisms (MM) in NF flow occurs [18]. The Fourier law has been used to study the issue of heat transmission, which has proven difficult to comprehend. Afterward—with Cattaneo and, later, Christov—an improved version of the Fourier law (FL) was created and applied to discuss and examine the issue of heat transfer through a stretching sheet [19–23]. Temperature and concentration characteristics are unaffected by the bioconvection factor [16], whereas the buoyancy parameter has an impact on the density and velocity of MM. Growing the magnetic field affects the NN—the nanoparticle concentration—and density of the MM [24–26], although solar energy has no impact on the density of MM [27]. As a result of the mass slip, the density of the MM, the heat, and the fluid flow are enhanced, whereas it modestly lowers the particle concentration [28,29]. The topic of this research is the investigation of the bioconvection mechanism across a stretched axisymmetric cylinder. The time-dependent temperature slipstream of NF, comprising MM along a flat tube, demonstrates that motivation energy has a significant impact on nanoparticle mobility inside conventional fluids [30]. The consequences of inner heat production or permeation on the heat/mass transport of NF comprising an MM across an inclined stretched axisymmetric cylinder have not been addressed in any earlier studies. The main objective of this exploration is to explore the impact of the incidence angle on the stream heat transfer, which is crucial in numerous industries such as in pipework, fiber optics, spherical plastic squeezing, the transition phase of conductive sheets, polyethylene production, and the condensation of electrical and automatic equipment. Shoaib et al. [31] investigated the numerical solution of magnetized hybrid nanofluids through a stretching sheet. Ullah et al. [32] studied the computational framework of MHD nanofluids with heat mass transmission over the vertical cone. Uddin et al. [33] used a neural network for investigating the thermal and chemical reactions of the thin-film movement of nanofluids according to their activation energy. Shoaib et al. [34] investigated the MHD flow of nanofluids passing through parallel plates numerically. Sabir et al. [35] explored the impact of Brownian motion on micropolar fluids with thermophoretic diffusion of nanoparticles.

The fluid that flows upon a rotating axisymmetric cylinder holds a significant position in many industrial requests, which appear widely in the area of aerodynamic systems, rotating machinery, and power-generating systems. One of the conventional problems of spinning surfaces in fluid mechanics is the rotating axisymmetric cylinder, which has been examined by various researchers considering different kinds of fluids in the form of the Newtonian class and non-Newtonian classes. From all of the rotating devices, it has been perceived that large values of the rotation factor heighten the fluid motion. Relevant work can also be seen in [36–40]. The neural networking strategy and error estimation have been performed by the researchers in [41]. Sowmya et al. [42] investigated the variation of temperatures with the thermal effect in an annular fin. Krishnamurthy et al. [43] performed a numerical analysis of the electric force on Newtonian fluids with periodic force.

In the present study, a numerical investigation of bioconvective nanofluid (NF) flow in gyrotactic microbes under convective boundary conditions (CBC)—involving a heat and mass transmission analysis—above an inclined extending axisymmetric cylinder is carried out. Via appropriate transformation, the set of Partial Differential Equations is transformed into a scheme of nonlinear ODEs. A new set of variables is presented in the directive to get the first-order convectional equations and then solved numerically using the built-in bvp4c MATLAB function. The error estimation is calculated and the obtained residual error validates the proposed model. The influence of several factors on the velocity, energy, concentration, and density of the motile microorganisms is investigated and examined. The analysis describes and addresses all physical measures of concentration such as Skin Friction (SF), the Sherwood number, the density of the motile microorganisms, and the Nusselt number. For validation of the present study, a comparison is carried out with previous studies. Furthermore, for confirmation of the bvp4c function, the ND-Solve approach is also applied. An error analysis is also performed for the confirmation of the mathematical model.

The following are the existing work's contributions: (a)—The temperature and velocity of NF are explored across a stretched inclined axisymmetric cylinder containing microorganisms; (b)—Using a proper transformation matrix, the set of PDEs are turned into ODEs; (c)—The resulting ODEs are investigated numerically using bvp4c, using Mathematica software9; (d)—The impact of various factors on the movement, heat, nanoparticle concentration, and DMM is shown visually.

In industrial applications, nanofluids are used to progress the proficiency of heat-transfer systems, which can lead to significant energy savings. In biomedical engineering, nanofluids have been used to develop new diagnostic and therapeutic techniques, such as targeted drug delivery systems. This study can be extended by adding Stefan blowing and multiple slip effects.

2. Mathematical Description

Consider a steady-state, uniform, mixed convection NF movement past an inclined, stretchable, axisymmetric cylinder with velocity U_w having radius a, containing GM (Gyrotacticn Microorganism), as described in Figure 1. The coordinates $(x;\ r)$ are used for this purpose. In Figure 1 T_w is the surface heat, T is the fluid heat, T_∞ $(T_w > T_\infty)$ is the ambient heat, and Q_0 is the heat source subjected to the axisymmetric cylinder.

When an axisymmetric cylinder is immersed in an NF, a temperature difference may arise between the surface of the axisymmetric cylinder and the surrounding fluid. This temperature difference can create a buoyancy force (BF) due to the density difference between the warm and cool fluid. The warm fluid near the axisymmetric cylinder surface will become less dense and rise, while the cool fluid will sink, creating a convective flow. This flow is known as natural convection and is driven by the BF, owing to the heat difference. In the presence of gravity, the BF—owing to the temperature difference—interacts with the gravitational force, resulting in a more complex flow pattern. The resulting flow can enhance heat transmission from the axisymmetric cylinder surface to the fluid, which can be beneficial in many engineering applications.

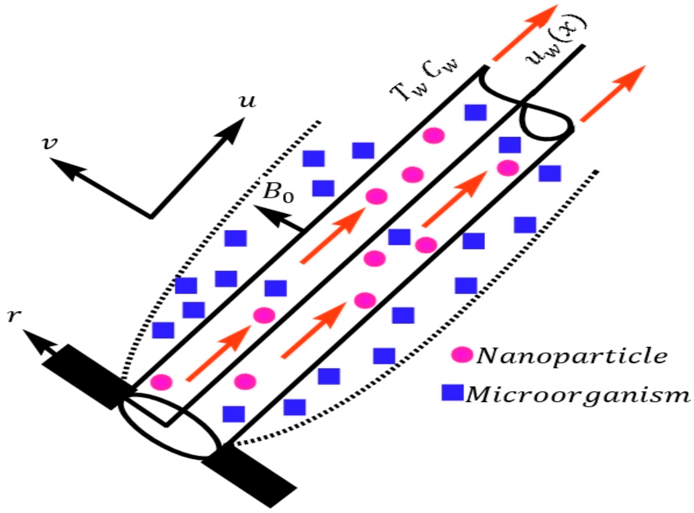

Figure 1. Configuration of the geometry and coordinates.

Ignoring pressure gradients or external forces, the model equations are expressed as follows [16–19,36–40]:

$$\frac{\partial}{\partial x}(ru)+\frac{\partial}{\partial r}(rv)=0 \tag{1}$$

$$\rho_{f\infty}\left(u\frac{\partial u}{\partial x}+v\frac{\partial u}{\partial r}\right)-\mu\left(\frac{1}{r}\frac{\partial}{\partial r}\left(r\frac{\partial u}{\partial r}\right)\right)-(1-C_\infty)\rho_{f\infty}\beta g(T-T_\infty)\cos\alpha_1+ \\ \left(\rho_p-\rho_{f\infty}\right)g(C-C_\infty)\cos\alpha_1+\left(\rho_{n\infty}-\rho_{f\infty}\right)g\gamma_1(n-n_\infty)\cos\alpha_1=0 \tag{2}$$

$$u\frac{\partial T}{\partial x}+v\frac{\partial T}{\partial r}=\frac{v}{\mu}\frac{1}{r}\frac{\partial}{\partial r}\left(r\frac{\partial T}{\partial r}\right)+\tau\left[\begin{array}{c} D_B\left(\frac{\partial T}{\partial r}\frac{\partial C}{\partial r}+\frac{\partial T}{\partial x}\frac{\partial C}{\partial x}\right)+ \\ \frac{D_T}{T_\infty}\left(\left(\frac{\partial T}{\partial r}\right)^2+\left(\frac{\partial T}{\partial x}\right)^2\right)\end{array}\right]+Q_0(T-T_\infty) \tag{3}$$

$$u\frac{\partial C}{\partial x}+v\frac{\partial C}{\partial r}=\frac{D_B}{r}\frac{\partial}{\partial r}\left(r\frac{\partial C}{\partial r}\right)+\frac{D_T}{T_\infty}\frac{1}{r}\frac{\partial}{\partial x}\left(r\frac{\partial C}{\partial r}\right) \tag{4}$$

$$u\frac{\partial n}{\partial x}+v\frac{\partial n}{\partial r}=\frac{D_n}{r}\frac{\partial}{\partial r}\left(r\frac{\partial n}{\partial r}\right)-\frac{b_cW_c}{(C_w-C_\infty)}\frac{1}{r}\frac{\partial}{\partial r}n\left(r\frac{\partial C}{\partial r}\right) \tag{5}$$

With boundary Constraints at:

$$r=a:\ u=U_w=U_0(x/l),\ v=0,\ T=T_w,\ C=C_w \tag{6}$$

$$n=n_w \text{ as } r\to\infty:\ u\to 0,\ v\to 0,\ T\to T_\infty,\ C\to C_\infty,\ n\to n_\infty \tag{7}$$

Equations (1)–(4) are, respectively, the continuity, movement, energy, and concentration equations. Where u and v are the x- and r-component of the velocity, ρ_{fx}, ρ_γ, ρ_{nx} are indeed the density of the fluid, nanomaterial, and microbes, correspondingly. Here, C explores the concentration profile, β is the capacity growth liquid coefficient, g is the gravity, α shows an angle of preference, γ_1 depicts the mean volume of the microbes, n is the DMM, T represents the hotness of the liquid, μ, v are the dynamic and kinematic viscosity, respectively, τ is the actual heat capacitance, D_y depicts the BM coefficient, D_r shows the thermophoresis measurement, D_n is the diffusivity of the microbes, b_c stands for the Chemotaxis constant, and W_c is the constant maximum cell swimming speed.

The relevant non-dimensional conversion

$$\eta = \frac{(r^2 - a^2)}{2a}\sqrt{\frac{U_w}{vx}}, u = a\sqrt{vU_w x f}(\eta), \theta(\eta) = \frac{T - T_\infty}{T_w - T_\infty}, \phi(\eta) = \frac{C - C_\infty}{C_w - C_\infty}, \chi = \frac{n - n_\infty}{n_w - n_\infty}. \tag{8}$$

is applied to simplify the set of mathematical equations.

The transformed equations in the ODEs are:

$$(2\gamma\eta + 1)f''' + (2\gamma + f)f'' f'^2 + R\ddot{i}[\theta - N_r\phi - R_b\chi]\cos\alpha_1 = 0 \tag{9}$$

$$(2\gamma\eta + 1)\theta'' + (2\gamma + \mathrm{Pr}f)\theta' + (2\gamma\eta + 1)\mathrm{Pr}\left[N_B\phi' + N_T\theta'\right]\theta' + \mathrm{Pr}\zeta\theta = 0 \tag{10}$$

$$(2\gamma\eta + 1)N_B\phi'' + N_B\left[2\gamma + Scf\right]\phi' + N_T\left[(2\gamma\eta + 1)\theta'' + 2\gamma\theta'\right] = 0 \tag{11}$$

$$(2\gamma\eta + 1)\chi'' + 2\gamma\chi' + Lb\mathrm{Pr}f\chi' - \mathrm{Pe}\begin{bmatrix} \sigma\gamma\phi' + \sigma(2\gamma\eta + 1)\phi'' + \gamma\phi'\chi \\ +(2\gamma\eta + 1)\phi''\chi + (2\gamma\eta + 1)\phi'\chi \end{bmatrix} = 0 \tag{12}$$

with the boundary constraints:

$$\begin{array}{l} f(0) = 0,\ f'(0) = 1,\ \theta(0) = 1,\ \phi(0) = 1,\ \chi(0) = 1, \\ \eta \to \infty:\ f' \to 0,\ \theta \to 0,\ \phi \to 0,\ \chi \to 0. \end{array} \tag{13}$$

Here,

$y = \frac{1}{a}\sqrt{\frac{vl}{U_0}}$ is the curvature factor,
$Ri = Gr_x/Re_x^2 = g\beta_T l^2/(xU_0^2)$ is Richardson's number,
$N_r = \frac{(\rho_p - \rho_\infty)\Delta C}{(1 - C_\infty)\beta\Delta T}$ is the Buoyancy ratio factor,
$Pr = v/\alpha$ is the Prandtl number,
$Rd = \frac{(\rho_{m\infty} - \rho_\infty)\gamma\Delta n}{(1 - C_\infty)\rho_\infty\beta\Delta T}$ is the bioconvection Rayleigh number,
$N_b = \tau D_B\Delta C/(vT_\infty)$ is the Brownian motion factor,
$N_t = \tau D_T\Delta T/(v\mathrm{T}_\infty)$ is the thermophoresis factor,
$\zeta = Q_0 l/\left(\rho C_p U_0\right)$ is the heat generation/absorption factor,
$Sc = v/D_B$ is the Schmidt number,
$B_L = D_B/D_n$ is the bioconvection Lewis number,
Pe is the Peclet number,
and $\sigma = n_\infty/(n_w - n_\infty)$ is the motile factor.

3. Physical Quantities (Skin Friction (SF), Nusselt Number (NN), and Sherwood Number (SN))

The dimensionless physical quantity of concentrations, such as the SF, NN, and SN, is given below:

$$\frac{1}{2}C_f\sqrt{\mathrm{Re}_x} = -f''(0), \frac{Nu_x}{\sqrt{\mathrm{Re}_x}} = -\theta'(0), \frac{Sh_x}{\sqrt{\mathrm{Re}_x}} = -\phi'(0), \frac{Nn_x}{\sqrt{\mathrm{Re}_x}} = -\chi'(0). \tag{14}$$

4. Results and Discussion

The basic flow equations were converted in terms of PDEs. The PDEs were transformed into dimensionless forms in terms of ODEs by using similarity transformations.

The numerical results were obtained using bvp4c with a 10^{-6} tolerance. For the verification of the bvp4c function, the ND-solve package was also applied, and a good correlation was established—as depicted in Figure 2a–d. Figure 2e represents the procedure of the bvp4c. Additionally, the existing work was compared with previous works, as explored in Table 1. The calculation in Table 1 delivered an excellent clearance for $-f''(0)$ and $-\theta'(0)$ between the present and previously published work.

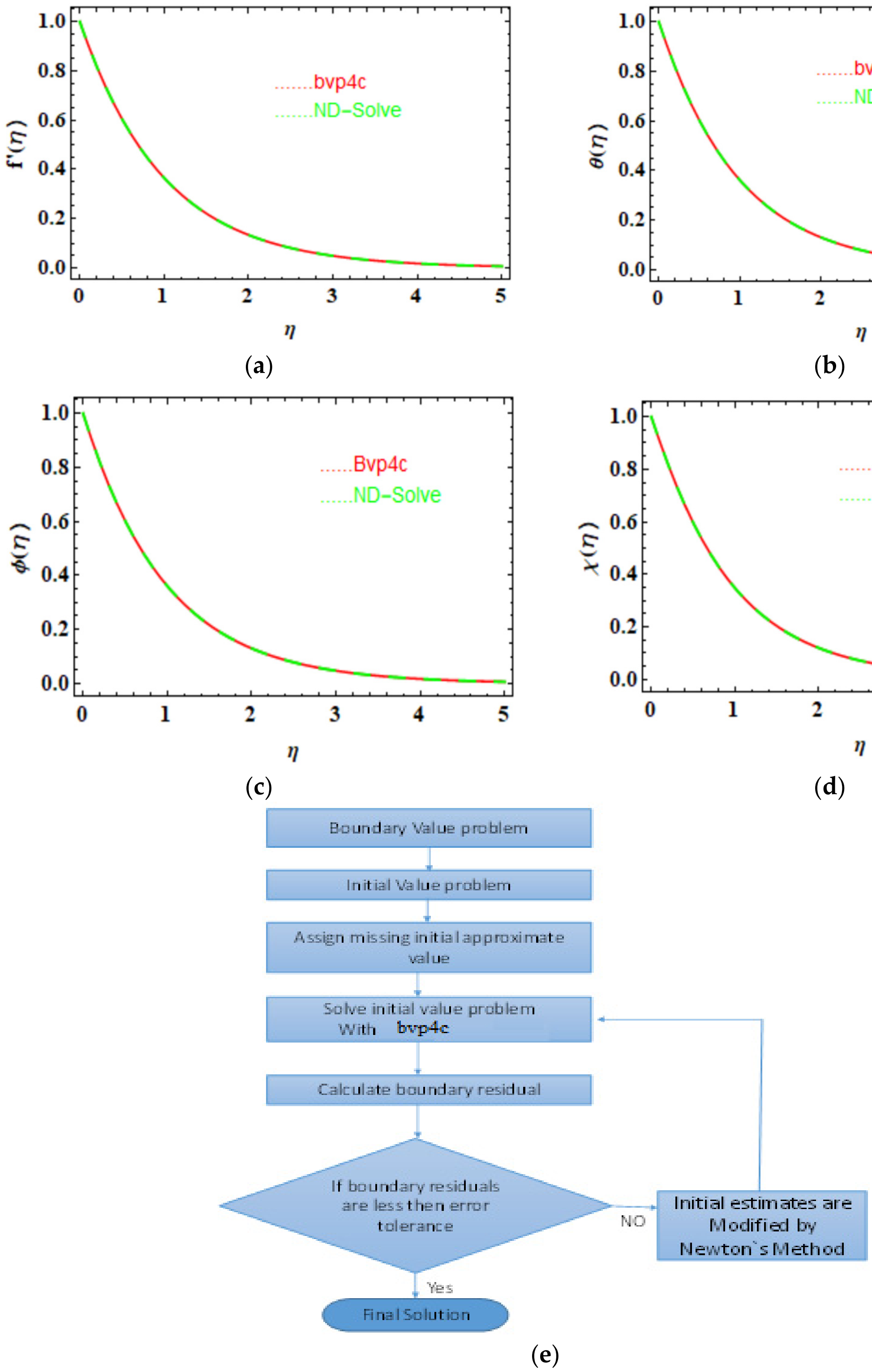

Figure 2. (**a**–**e**) Assessment of bvph4c and ND-solve for $f'(\eta)$ and $\theta(\eta)$. $\phi(\eta)$ and $\chi(\eta)$; Flow chart of bvp4c.

Table 1. Impression of the physical parameter Pr on the physical quantities of interest and their confirmation.

	Present Work		Wang [6]	
Pr	$-f''(0)$	$-\theta'(0)$	$-f''(0)$	$-\theta'(0)$
0.2	1.4338	0.2701996	1.4331	0.2702
0.6	1.4328	0.5640398	1.4323	0.5640
2	1.4299	0.8224698	1.4298	0.8225
6	1.4285	2.9064991	1.4280	2.9065
15	1.4163	4.4648811	1.4157	4.4649
20	1.4042	7.57322885	1.4035	7.5733

The dimensionless first-order differential equations were solved using the bvp4c package; it was implemented using various software packages such as MATLAB and Mathematica. By default, these packages use a certain working precision, which determines the accuracy of the numerical solution. Since we were interested in a numerical solution, the error estimations for the parameters were essential. The error was computed based on the difference between two different precisions, i.e., the default work precision and working precision–22. Indeed, logarithmic scales are often used to visualize small differences or changes that can span several orders of magnitude. By taking the logarithm of a variable, you compress its range of values and emphasize differences in the lower end of the scale, where they might otherwise be difficult to discern. In the case of real exponents [x], taking the logarithm base 10 of the absolute value of the exponent can be a useful transformation; this is because the absolute value ensures that the logarithm is always defined, even when the exponent is negative or zero. By using a logarithmic scale, you can compare values that differ by orders of magnitude, while still being able to see small differences near zero. In the figures below, we computed the error solutions for various physical model factors. Based on these estimates, our numerical answer was correct, as the error was small—as seen in Figures 3a–d and 4a–d. The bioconvection Lewis factor B_L indicates the ratio of thermal diffusivity towards the diffusivity of microorganisms. The B_L had no influence on the Skin friction, Nusselt Number, or Sherwood Number, as seen in Table 2. There was an upsurge in DMM. By raising the B_L quantity, the DMM declined (see Figure 5a).

Table 2. Influence of B_L on $-f''(0)$, $-\theta'(0)$, $-\phi'(0)$, and $-\chi'(0)$.

$\boldsymbol{B_L}$	$\mathbf{-f''(0)}$	$\boldsymbol{-\theta'(0)}$	$\boldsymbol{-\phi'(0)}$	$\boldsymbol{-\chi'(0)}$
0.2	1.4338	0.2701	1.3266	1.6137
0.4	1.4338	0.2701	1.3266	1.7344
0.6	1.4338	0.2701	1.3266	1.8235
0.8	1.4338	0.2701	1.3266	1.8610

Physically raising B_L reduces the diffusivity of microorganisms. Brownian motion, N_b, denotes the molecular movement of deferred nanomaterials inside an NF. This movement is caused by the random movement of nanoparticles, which becomes more prominent as the temperature rises. Table 3 reveals that the N_b had no effect on the SF or DMM, although it did reduce the NN (heat transfer by conduction).

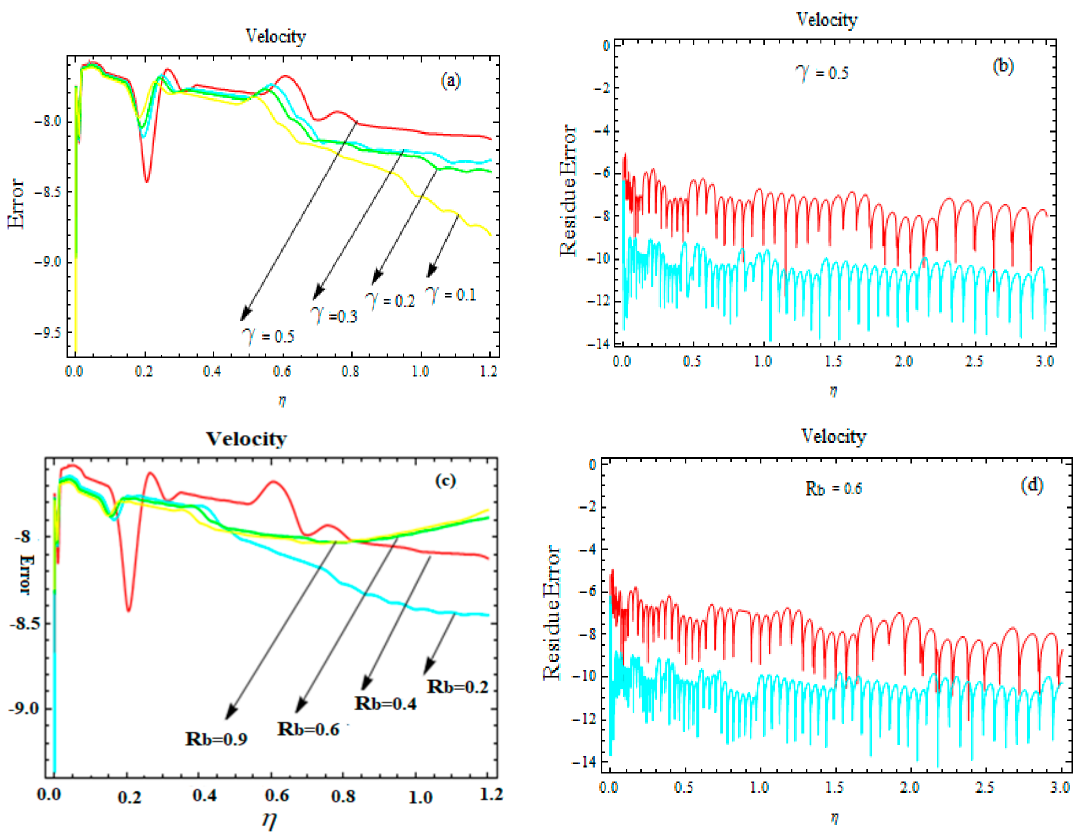

Figure 3. (**a**–**d**) Error estimation for the velocity profile for different values of γ and R_i.

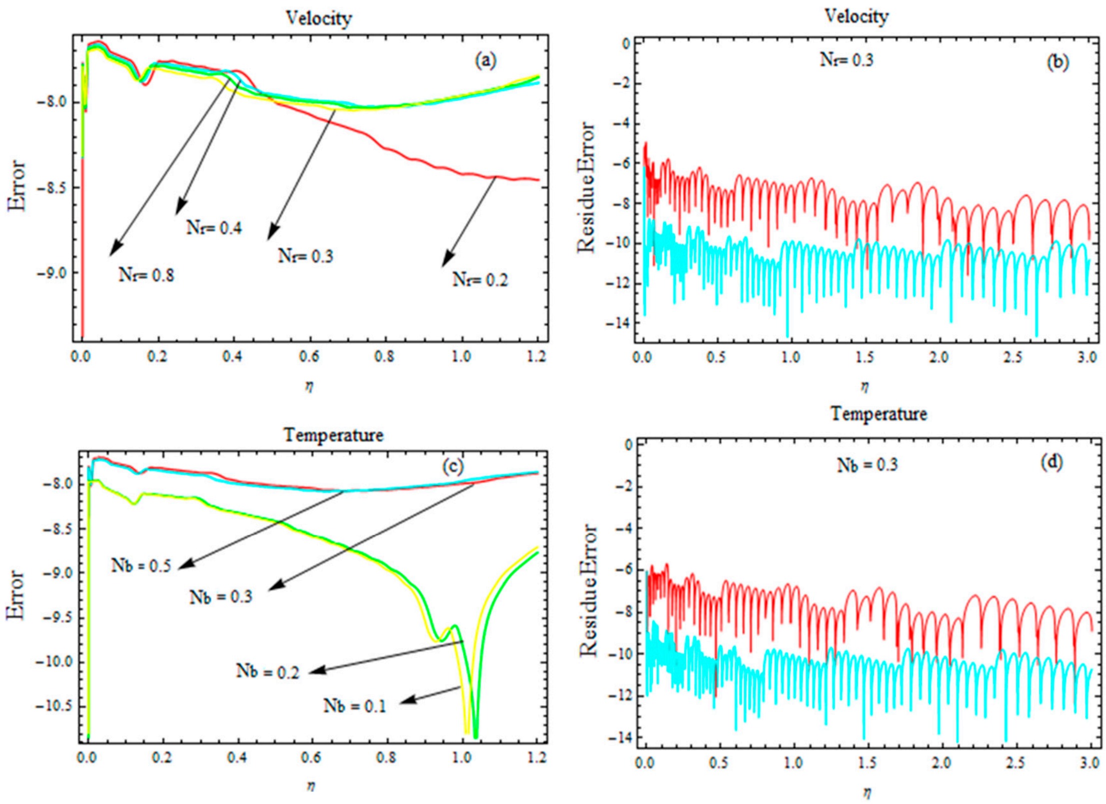

Figure 4. (**a**–**d**) Error estimation for the velocity and temperature profiles with different values of $\boldsymbol{N_r}$ and $\boldsymbol{N_b}$.

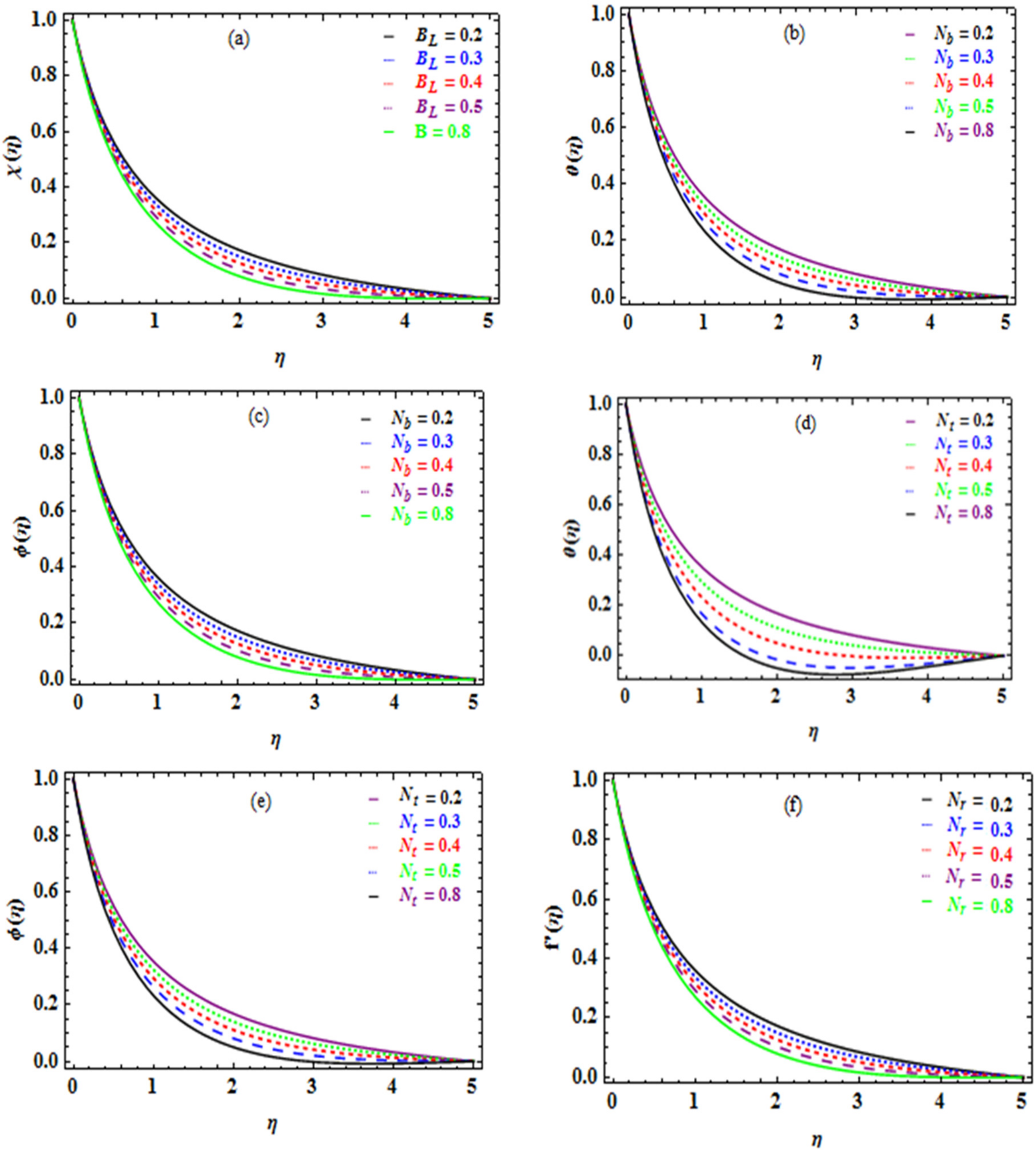

Figure 5. Influence of (**a**) B_L on $\chi(\eta)$, (**b**). N_b on $\theta(\eta)$, (**c**) N_b on $\phi(\eta)$, (**d**) N_t on $\theta(\eta)$, (**e**) N_t on $\phi(\eta)$, (**f**) N_t on $f'(\eta)$.

Table 3. Influence of N_b on $-f''(0)$, $-\theta'(0)$, $-\phi'(0)$ and $-\chi'(0)$.

N_b	$-f''(0)$	$-\theta'(0)$	$-\phi'(0)$	$-\chi'(0)$
0.2	1.4353	0.6406	1.2765	0.7626
0.4	1.4343	0.6106	1.3173	0.7686
0.6	1.4328	0.5469	1.3479	0.7733
0.8	1.4299	0.3976	1.3657	0.7768

Figure 5b–c shows how N_b affected the temperature and concentration profiles. It was observed that the temperature outline was enhanced (see Figure 5b), while the concentration declined (see Figure 5c). Table 4 demonstrates an escalation in the concentration of the

microchannel. Figure 5c depicts a drop in the concentration of nanoparticles far from the surface. Physically, the temperature was enhanced, accelerating the energy of the particles, which promoted more motion and faster collisions, which enhanced Brownian motion. While raising the concentration, the space for particle mobility was reduced, as it decreased the possibility of collisions.

Table 4. Influence of N_t on $-f''(0)$, $-\theta'(0)$, $-\phi'(0)$, and $-\chi'(0)$.

N_t	$-f''(0)$	$-\theta'(0)$	$-\phi'(0)$	$-\chi'(0)$
0.2	1.4338	0.5985	1.3331	0.9718
0.4	1.4328	0.5469	1.3479	0.9733
0.6	1.4291	0.4773	1.4244	0.9828
0.8	1.4252	0.4357	1.5063	0.9933

The thermophoresis factor N_t refers to the phenomena of a nanoparticle disparity reaction due to the force of a heat variation. The TR gradient enhances this force, which enhances the heat inside the flow (see Figure 5d). It was observed that the concentration of the nanoparticles rose (see Figure 5e). Table 4 demonstrates the influence of N_t on the SF, NN, SN, and DMM. This table demonstrated a drop in the NN with N_t, followed by a rise in the thermal gradient—as shown in Figure 5d. Table 4 indicates a rise in the Sherwood number, and Figure 5b indicates an increase in the nanoparticle concentration. Physically, raising the temperature raised the temperature gradients, which raised the transition force and thus raised the convective heat transfer parameter.

Here, N_r is the buoyancy-ratio factor. Table 5 shows that raising the N_r factor led to an increase in SF and a reduction throughout the NN, SN, and DMM. Figures 5f and 6a–c depict the influence of N_r. The velocity of MM decreased (see Figure 5f), whereas the temperature, boundary layer flow concentration, and DMM rose—as shown in Figure 6a–c, respectively.

Table 5. Influence of N_r on $-f''(0)$, $-\theta'(0)$, $-\phi'(0)$, and $-\chi'(0)$.

N_r	$-f''(0)$	$-\theta'(0)$	$-\phi'(0)$	$-\chi'(0)$
0.0	1.2812	0.3915	1.4674	1.6529
0.4	1.3351	0.3859	1.4486	1.6375
0.6	1.3726	0.3714	1.4339	1.6257
1.0	1.4727	0.3622	1.3867	1.5885

The Peclet number, Pe, is the proportion of the advective transportation rate versus the mass diffusion rate. Table 6 indicates that when the Pe number increased, so did the concentration of MM, while no significant effect was observed for the SF, NN, and SN. Figure 6d depicts a decline in the fields of motile microorganisms as the Pe number increased.

Table 6. Influence of Pe on $-f''(0)$, $-\theta'(0)$, $-\phi'(0)$, and $-\chi'(0)$.

Pe	$-f''(0)$	$-\theta'(0)$	$-\phi'(0)$	$-\chi'(0)$
0.0	1.4443	0.3721	1.4266	1.6137
0.4	1.4442	0.3721	1.4267	1.9147
0.6	1.4441	0.3721	1.4267	3.2163
1.0	1.4439	0.3722	1.4268	3.5186

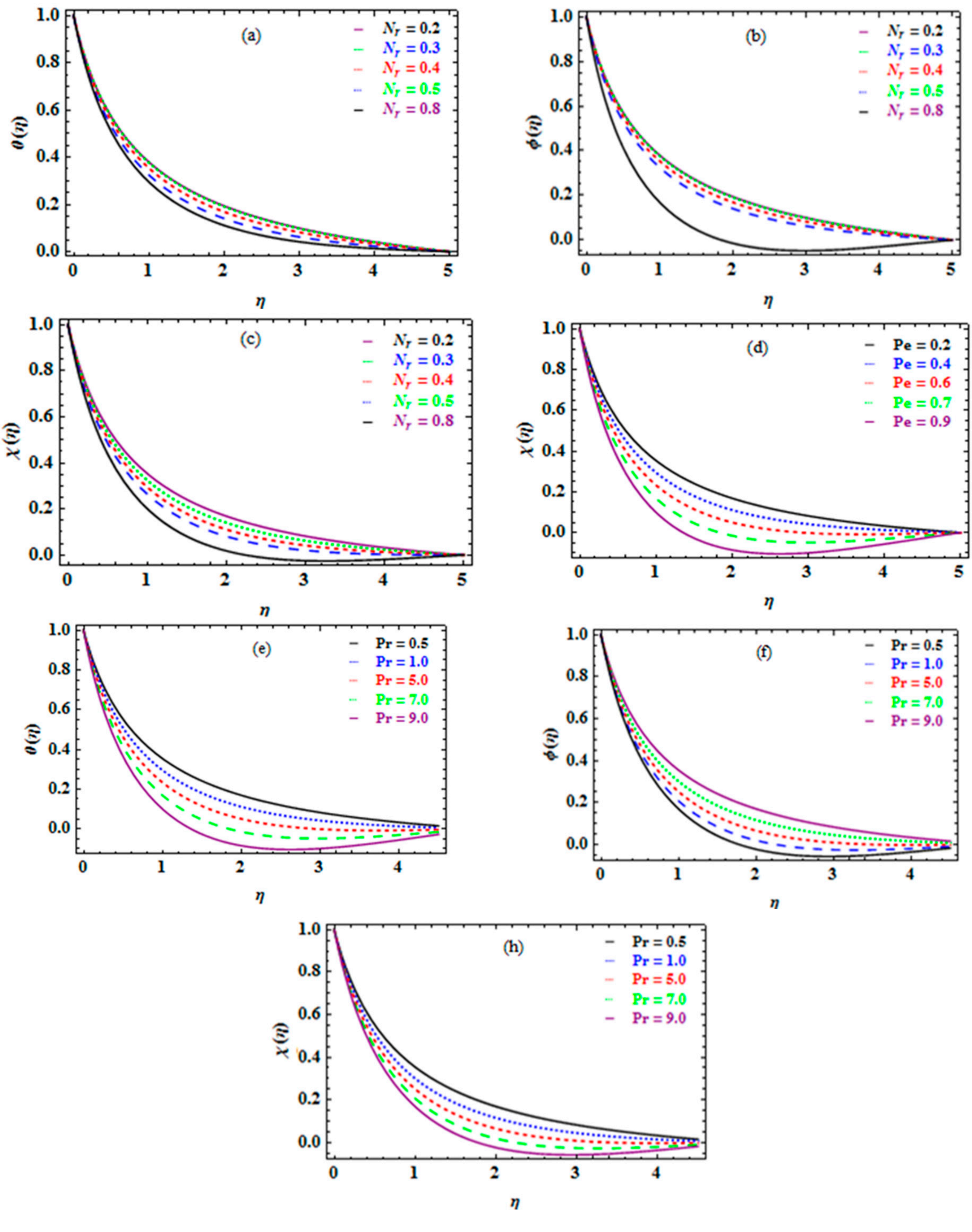

Figure 6. Influence of (**a**) N_r on $\theta(\eta)$, (**b**) N_r on $\phi(\eta)$, (**c**) N_r on $\chi(\eta)$, (**d**) Pe on $\theta(\eta)$, (**e**) Pr on $\theta(\eta)$, (**f**) Pr on $\phi(\eta)$, (**h**) Pr on $\chi(\eta)$.

The Prandtl number, Pr, is indeed a nondimensional quantity that shows the relationship between the momentum diffusivity and the thermal diffusivity. This value compares the influence of the fluid viscosity to the associated heat conductivity. The magnitude of the

Pr number describes the characteristics of the fluid under investigation. Heat-transmitting fluids have a strong heat capacity as well as low *Pr* values. According to Table 7, raising the *Pr* number has little impact on skin friction, but improves the Nusselt number, Sherwood number, and DMM. If $Pr = 0.7$, the air may be designated a heat transmission fluid. Carbon disulfide has a viscosity of 0.5 and a thermal conductivity of 0.149. The *Pr* for chloromethane is five and for water is seven. As the *Pr* number grows, the impact of viscosity increases and the temperature rises, while the concentration declines. Figure 6d–f depict the effects of *Pr*. The heat is shown to be decreasing in Figure 6d. Physically, a rise in *Pr* number indicates a reduction in heat flux, implying that the solvent has a higher heat capacity. Figure 6e demonstrates that the concentration of the microchannel rose further from the substrate, but also that the DMM decreased (see Figure 6f).

Table 7. Influence of *Pr* on $-f''(0)$, $-\theta'(0)$, $-\phi'(0)$, and $-\chi'(0)$.

Pr	$-\mathbf{f}''(\mathbf{0})$	$-\theta'(\mathbf{0})$	$-\phi'(\mathbf{0})$	$-\chi'(\mathbf{0})$
0.5	1.4313	0.5549	1.3463	0.9142
2	1.4379	0.5285	1.3556	1.1583
6	1.4442	0.3721	1.4266	1.6137
8	1.4452	0.2539	1.4746	1.8496

The Bioconvection Rayleigh Number, R_b, reflects the heat transmission in MM by natural convection. With rising R_b numbers, there was an improvement in SF but a decline in the NN, SN, and DMM. Figure 7a depicts a reduction in the velocity distribution as R_b increased. In addition, Figure 7b–d coincide with Table 8 and show a rise in temperature, nanoparticle concentration, and motile microorganism performance when R_b is increased.

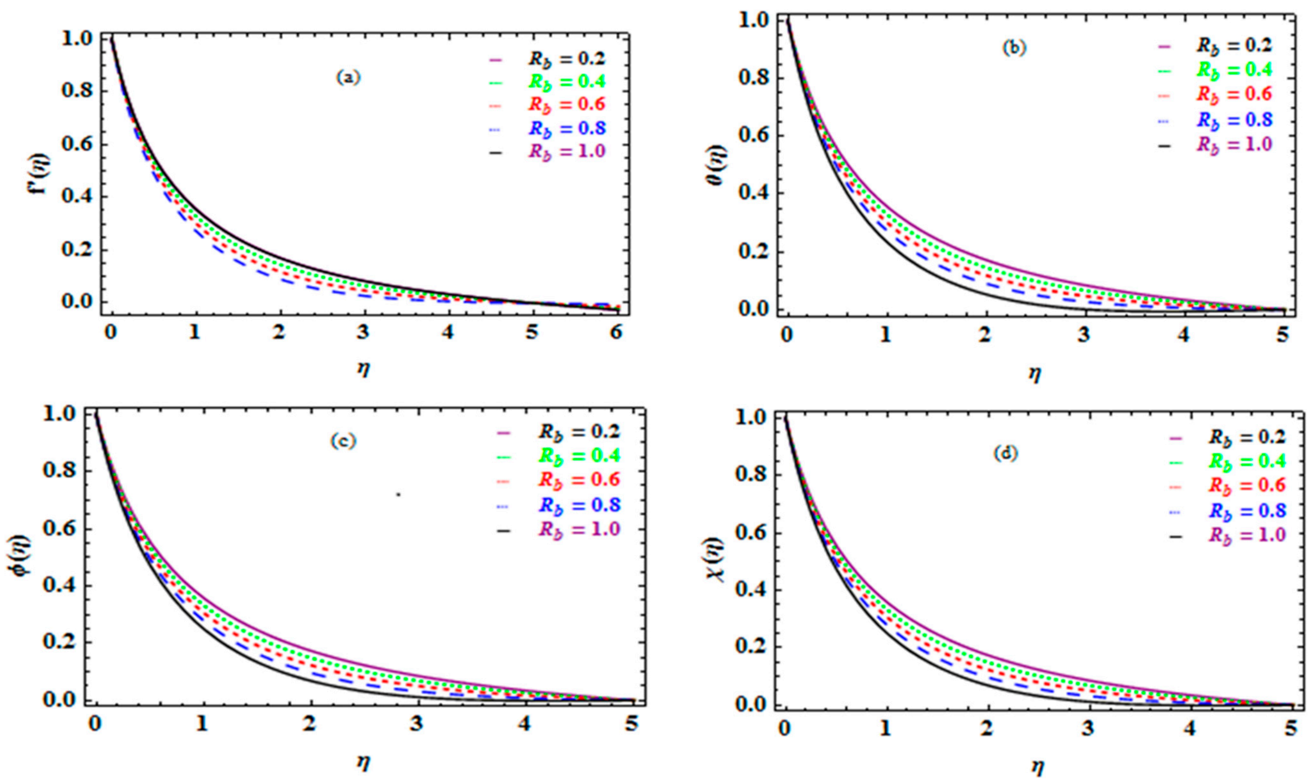

Figure 7. (**a**–**d**) Influence of R_b.

Table 8. Influence of R_b on $-f''(0)$, $-\theta'(0)$, $-\phi'(0)$, and $-\chi'(0)$.

R_b	$-f''(0)$	$-\theta'(0)$	$-\phi'(0)$	$-\chi'(0)$
0.0	1.3218	0.3872	1.4516	1.6393
0.2	1.3351	0.3859	1.4486	1.6375
0.6	1.3888	0.3792	1.4362	1.6258
1.0	1.4579	0.3719	1.4189	1.5998

The Richardson number, R_i, is a non-dimensional quantity that represents the buoyancy component to the stream-sheared ratio. Table 9 illustrates that raising the R_i increased the SF, NN, SN, and DMM. Figure 8a–d demonstrates a drop in the curves of the velocity, temperature, boundary layer flow concentration, and DMM when R_i was increased.

Table 9. Influence of R_i on $-f''(0)$, $-\theta'(0)$, $-\phi'(0)$, and $-\chi'(0)$.

R_i	$-f''(0)$	$-\theta'(0)$	$-\phi'(0)$	$-\chi'(0)$
1.0	1.3218	0.3859	1.4486	1.6375
1.6	1.3351	0.3878	1.4682	1.6591
2.5	1.3888	0.3977	1.4846	1.6776
5.0	1.4579	0.4164	1.4988	1.6839

The Schmidt number, Sc, is the relationship between the kinematic viscosity and the mass diffusion. Table 10 depicts the impact of Sc; a drop in the NN and an enhancement of SN. Figure 8e,f illustrates the increase in the temperature distribution and a reduction in the nanoparticle concentration with rising Sc numbers. In terms of physics, raising the Schmidt number enormously increased the dynamic viscosity of the density of the fluid with mass diffusivity, which increased the thickness of the mass transmission boundary layer. The proposed value for Sc in the current investigation is very small, indicating that the molecules had a strong diffusivity, were extremely small, and were unaffected by the viscosity of the media. Consequently, as the heat rose, so did the Sc number—whereas the concentration declined as the Sc increased.

Table 10. Influence of Sc on $-f''(0)$, $-\theta'(0)$, $-\phi'(0)$, and $-\chi'(0)$.

Sc	$-f''(0)$	$-\theta'(0)$	$-\phi'(0)$	$-\chi'(0)$
0.0	1.4551	0.7981	0.5134	1.4931
0.5	1.4533	0.7321	0.6242	1.5172
1.2	1.4498	0.6324	0.7869	1.5375
2.0	1.4443	0.3721	1.4266	1.6137

The effect of the angle of inclination is shown in Table 11 to demonstrate the variance in these non-dimensional values as a function of the inclination angle. Varying the inclination angle significantly influenced the movement, temperature, volume of the nanoparticles, and the DMM, as revealed in Figure 9a–d, respectively.

The curvature factor, γ, represents the distortion of the axisymmetric cylinder sheet according to the size of the boundary layer. The surface area declined as the curvature factor increased. Table 12 demonstrates an improvement in SF, NN, SN, and DMM as the curvature factor was increased, owing to a consequent reduction in area. Figure 9e–h explores how the curvature factor γ affected the velocity, temperature, and volume of the NF away from the surface, and the MM profiles. For $\gamma = 1$, the radius equalled the thickness of the boundary layer, and the structure was axisymmetric; as γ grew, we produced a slender axisymmetric cylinder with a dense boundary layer. The heat source factor ξ is a dimensionless factor that explores the quantity of heat created or absorbed in the medium. Table 13 shows that shifting the variation from absorption to generation caused a drop in the NN and a rise in the SN. The temperature as well as the concentration of the nanomaterial enhancement are seen in Figure 10a,b. Table 14 shows that the bioconvection factor σ caused a slight improvement in the DMM. Figure 10c reveals a small decline in the MM (motile microorganisms) as the bioconvection factor was increased.

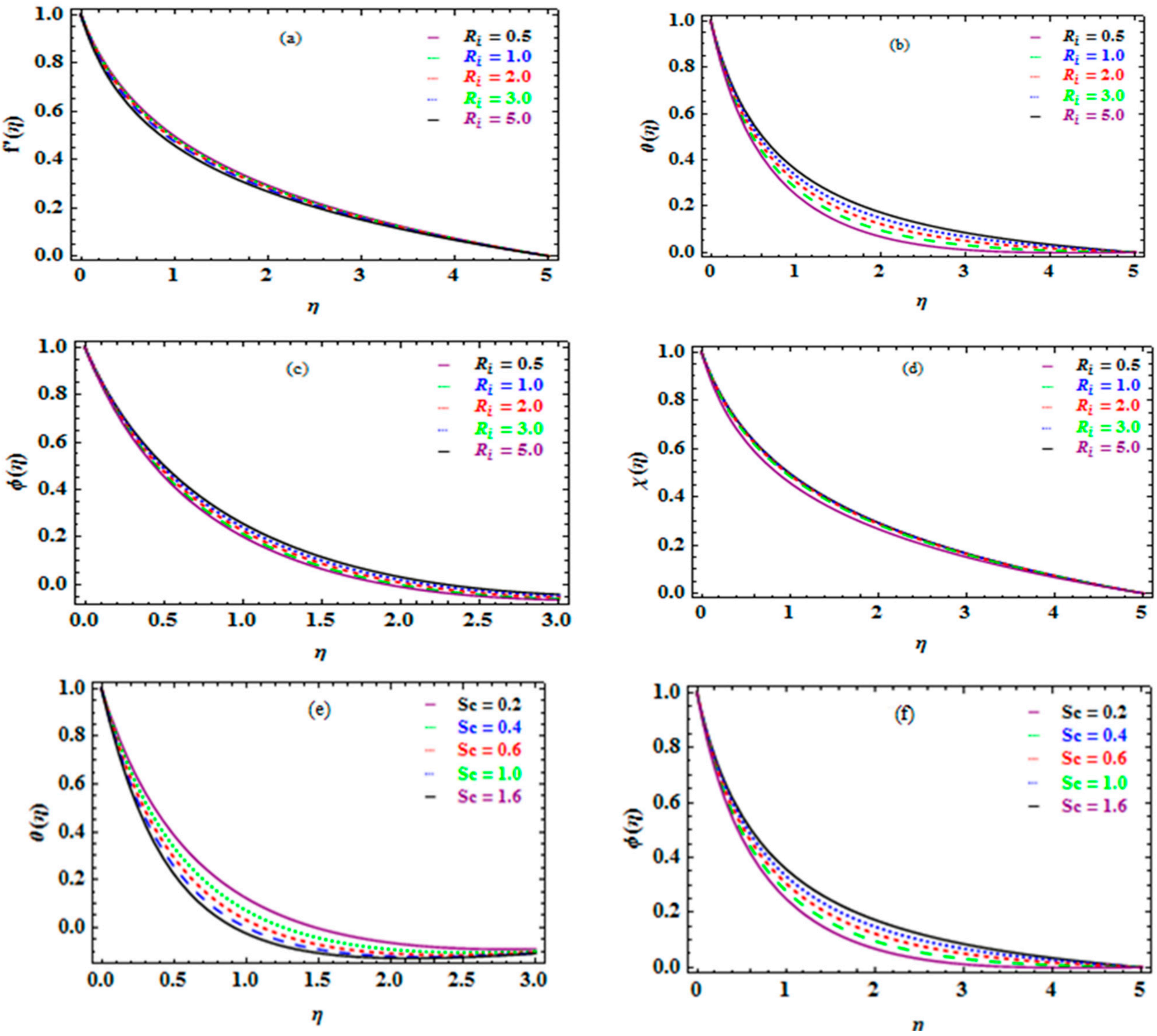

Figure 8. (**a**–**f**) Influence of R_i and Sc.

Table 11. Influence of α on $-f''(0)$, $-\theta'(0)$, $-\phi'(0)$, and $-\chi'(0)$.

$cos\alpha$	$-\mathbf{f}''(\mathbf{0})$	$-\theta'(\mathbf{0})$	$-\phi'(\mathbf{0})$	$-\chi'(\mathbf{0})$
0.0	1.4571	0.3693	1.4237	1.5997
0.3	1.3351	0.3859	1.4486	1.6375
0.7	1.4591	0.3738	1.3999	1.5976
0.86	1.4573	0.3698	1.4225	1.5995
1.0	1.4612	0.3748	1.3956	1.5963

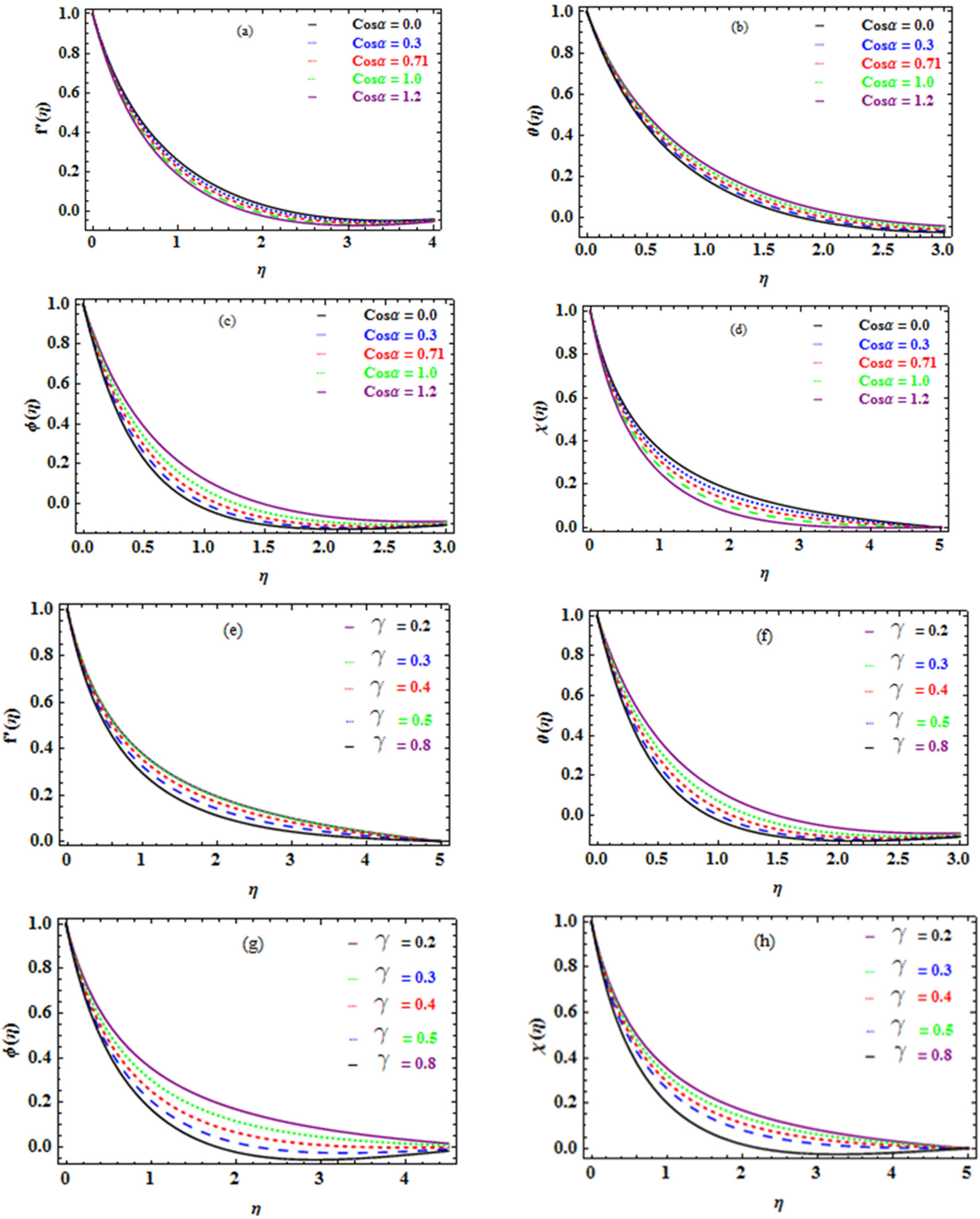

Figure 9. (**a**–**h**) Influence of $cos\alpha$ and γ.

Table 12. Influence of γ on $-f''(0)$, $-\theta'(0)$, $-\phi'(0)$, and $-\chi'(0)$.

γ	$-\mathbf{f}''(\mathbf{0})$	$-\theta'(\mathbf{0})$	$-\phi'(\mathbf{0})$	$-\chi'(\mathbf{0})$
1	1.4424	0.3778	1.4239	1.6147
2	1.9236	0.3623	2.1494	2.3147
4	2.5399	0.3591	2.8264	2.9697
6	2.9413	0.3717	3.5213	3.5994

Table 13. Influence of ξ on $-f''(0)$, $-\theta'(0)$, $-\phi'(0)$, and $-\chi'(0)$.

ξ	$-\mathbf{f}''(\mathbf{0})$	$-\theta'(\mathbf{0})$	$-\phi'(\mathbf{0})$	$-\chi'(\mathbf{0})$
−0.1	1.4485	0.7297	1.3164	1.5899
0.0	1.4469	0.5677	1.3675	1.5962
0.1	1.4443	0.3721	1.4266	1.6137
0.3	1.4379	0.1473	1.4988	1.6253

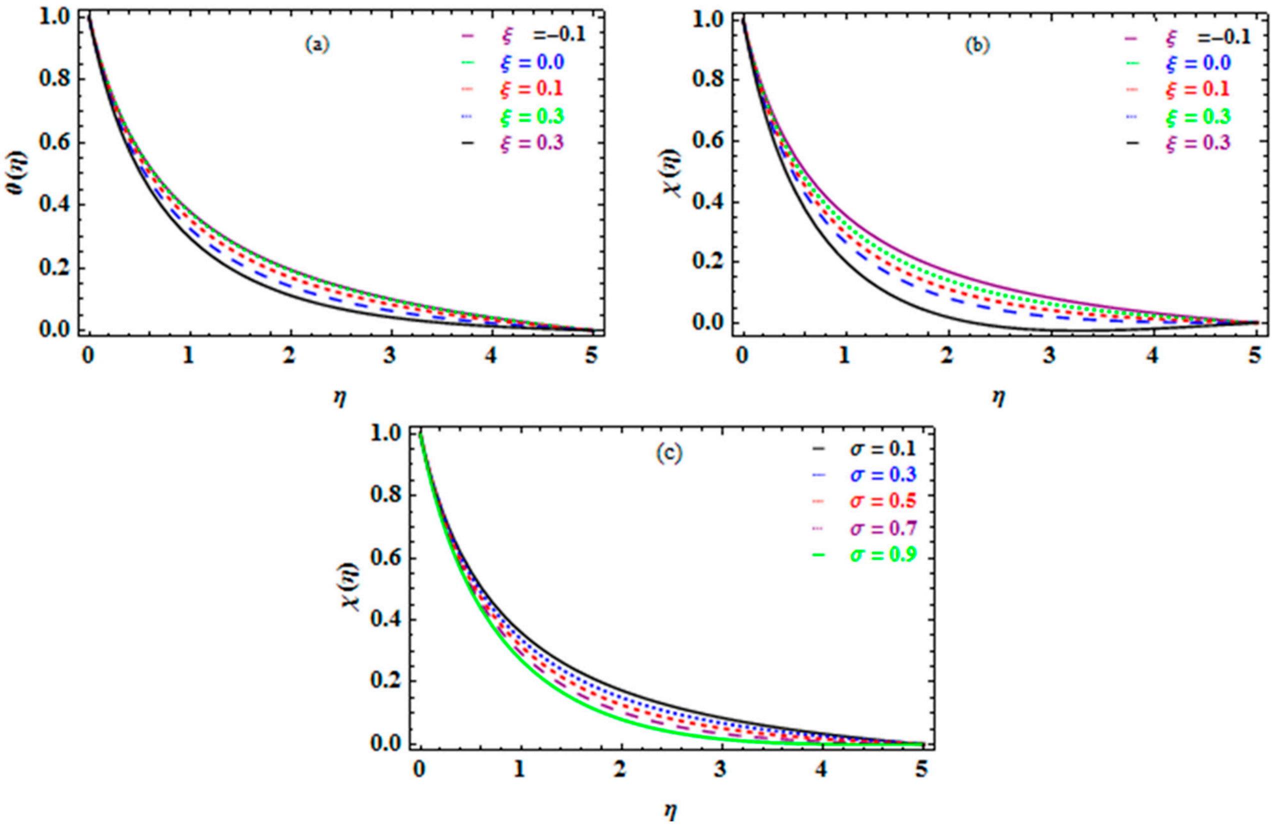

Figure 10. (**a**–**c**) Influence of ξ and σ.

Table 14. Influence of σ on $-f''(0)$, $-\theta'(0)$, $-\phi'(0)$, and $-\chi'(0)$.

σ	$-\mathbf{f}''(\mathbf{0})$	$-\theta'(\mathbf{0})$	$-\phi'(\mathbf{0})$	$-\chi'(\mathbf{0})$
0.1	1.4472	0.3678	1.4329	1.6134
0.3	1.4472	0.3678	1.4329	1.6383
0.6	1.4472	0.3678	1.4329	1.6633
0.9	1.4472	0.3678	1.4329	1.6882

5. Conclusions

The laminar movement of an NF through an inclined axisymmetric cylinder in the context of generation/absorption, bioconvection, and the presence of MM was investigated numerically. Through appropriate transformation, a network of PDEs was turned into a set of dimensionless ODEs, which were then computationally solved utilizing Mathematica Package bvp4c with an ND-solve approach. The simulation outcomes were consistent with earlier findings. It was observed that the SF rose as N_r and γ were enhanced, while it was diminished by increasing R_b and R_i. Furthermore, SF was not influenced by other factors. The NN grew by enhancing R_i and Sc. When B_L, Pe, and σ were changed, the NN remained constant, but when other factors were improved, the NN decreased. The SN was only increased by increasing buoyancy factor N_r. Although the SN was constant for B_L, Pe, R_b, R_i, and σ, the SN rose when the other factors were changed. It was observed that the DMM was reduced when N_r and R_b were enhanced and increased with other factors. On the other hand, the inclination angle had no impact. For angles < 45°, the SPF, NN, and SN rose, and they declined for angles > 45°. As the curvature factor γ was increased, so was the velocity distribution, while it declined when N_r and R_b were enhanced. It was detected that the temperature profile increased with growing values of BM, the Richardson number, and the Schmit number, while the bioconvection factor had no effect. In industrial applications, nanofluids are used to progress the proficiency of heat transfer systems, which can lead to significant energy savings. In biomedical engineering, nanofluids have been used to develop new diagnostic and therapeutic techniques, such as targeted drug delivery systems. This study can be extended by adding Stefan blowing and multiple slip effects.

Author Contributions: F.A.A. and T.G. wrote the manuscript, E.A.A.I., and T.G. modeled the problem, W.K., and A.S.K. solved the problem. T.G. and A.S.K., obtained the numerical computations. All authors have read and agreed to the published version of the manuscript.

Funding: Project number (RSPD2023R1060), King Saud University, Riyadh, Saudi Arabia.

Acknowledgments: Researcher Supporting Project number (RSPD2023R1060), King Saud University, Riyadh, Saudi Arabia.

Conflicts of Interest: The authors declare no conflict of interest.

Nomenclature

$(x;\ r)$	Coordinates	τ	Actual heat capacitance
T_w	Surface heat	D_{r}	Thermophoresis measurement
T	Fluid heat	D_y	Brownian motion coefficient
Q_0	Heat source	D_n	Diffusivity of the microbes
ρ_{fx}	Density of fluid	b_c	Chemotaxis constant
ρ_γ	Density of nanomaterial	W_c	Maximum cell swimming speed
ρ_{nx}	Density of microbes	y	Curvature factor
C	Concentration profile	Ri	Richardson's number
β	Capacity growth liquid coefficient	N_r	Buoyancy ratio factor
g	Gravity	Pr	Prandtl number
α	Angle of preference	Rd	Bioconvection Rayleigh number
γ_1	The mean volume of the microbes	N_b	Brownian motion factor
T	The hotness of the liquid	N_t	Thermophoresis factor
μ	Dynamic viscosity	ζ	Heat generation/absorption factor
v	Kinematic viscosity	Sc	Schmidt number
B_L	Bioconvection Lewis number	Pe	Peclet number
σ	Motile factor		

References

1. Anderson, J.D. Ludwig Prandtl's boundary layer. *Phys. Today* **2005**, *58*, 42–48. [CrossRef]
2. Sakiadis, B.C. Boundary-layer behavior on continuous solid surfaces: I. Boundary-layer equations for two-dimensional and axisymmetric flow. *AIChE J.* **1961**, *7*, 26–28. [CrossRef]
3. Sakiadis, B.C. Boundary-layer behavior on continuous solid surfaces: II. The boundary layer on a continuous flat surface. *AIChE J.* **1961**, *7*, 221–225. [CrossRef]
4. Crane, L.J. Flow past a stretching plate. *Z. Angew. Math. Phys. ZAMP* **1970**, *21*, 645–652. [CrossRef]
5. Dutta, B.K.; Roy, P.; Gupta, A.S. Temperature field in flow over a stretching sheet with uniform heat flux. *Int. Commun. Heat Mass Transfer* **1985**, *12*, 89–94. [CrossRef]
6. Wang, C.Y. Fluid flow due to a stretching axisymmetric cylinder. *Phys. Fluids* **1988**, *31*, 466–474. [CrossRef]
7. Ishak, A.; Nazar, R.; Pop, I. Uniform suction/blowing effect on flow and heat transfer due to a stretching axisymmetric cylinder. *Appl. Math. Model.* **2008**, *32*, 2059–2066. [CrossRef]
8. Choi, S.U.; Eastman, J.A. *Enhancing Thermal Conductivity of Fluids with Nanoparticles*; (No. ANL/MSD/CP-84938; CONF-951135-29); Argonne National Laboratory: Lemont, IL, USA, 1995.
9. Buongiorno, J. Convective transport in NFs. *J. Heat Transf.* **2006**, *128*, 240–250. [CrossRef]
10. Alanazi, M.M.; Hendi, A.A.; Raza, Q.; Rehman, M.A.; Qureshi, M.Z.A.; Ali, B.; Shah, N.A. Numerical computation of hybrid morphologies of nanoparticles on the dynamic of nanofluid: The case of blood-based fluid. *Axioms* **2023**, *12*, 163. [CrossRef]
11. Xian, H.W.; Sidik, N.A.C.; Najafi, G.J.J.O.T.A. Recent state of NF in automobile cooling systems. *J. Therm. Anal. Calorim.* **2019**, *135*, 981–1008. [CrossRef]
12. Sheikhpour, M.; Arabi, M.; Kasaeian, A. Role of NFs in drug delivery and biomedical technology: Methods and applications. *Nanotechnol. Sci. Appl.* **2020**, *13*, 47–59. [CrossRef]
13. Nagarajan, P.K.; Subramani, J.; Suyambazhahan, S. NFs for solar collector applications. *Energy Procedia* **2014**, *61*, 2416–2434. [CrossRef]
14. Mukhtar, S.; Gul, T. Solar Radiation and Thermal Convection of Hybrid Nanofluids for the Optimization of Solar Collector. *Mathematics* **2023**, *11*, 1175. [CrossRef]
15. Saidur, R.; Leong, K.Y.; Mohammed, H.A. A review on applications and challenges of NFs. *Renew. Sustain. Energy Rev.* **2011**, *15*, 1646–1668. [CrossRef]
16. Wong, K.V.; De Leon, O. Applications of NFs: Current and future. *Adv. Mech. Eng.* **2010**, *2*, 519659–519665. [CrossRef]
17. Sandeep, N.; Ashwinkumar, G.P. Impact of nanoparticle shape on magnetohydrodynamic stagnation-point flow of carreau nanoliquid: A comparative study. *Proc. Inst. Mech. Eng. Part E J. Process Mech. Eng.* **2021**, *9*, 544–556. [CrossRef]
18. Shahid, A.; Huang, H.; Bhatti, M.M.; Zhang, L.; Ellahi, R. Numerical investigation on the swimming of gyrotactic microorganisms in nanofluids through porous medium over a stretched surface. *Mathematics* **2020**, *8*, 380. [CrossRef]
19. Anjum, N.; Khan, W.A.; Azam, M.; Ali, M.; Waqas, M.; Hussain, I. Significance of bioconvection analysis for thermally stratified 3D Cross nanofluid flow with gyrotactic microorganisms and activation energy aspects. *Therm. Sci. Eng. Prog.* **2012**, *38*, 101596. [CrossRef]
20. Acharya, N.; Das, K.; Kundu, P.K. Framing the effects of solar radiation on magneto-hydrodynamics bioconvection NF flow in presence of gyrotactic microorganisms. *J. Mol. Liq.* **2016**, *222*, 28–37. [CrossRef]
21. Uddin, M.J.; Yasser, A.O.; Bég, A.; Kabir, M.N. Numerical solutions for gyrotactic bioconvection in NF-saturated porous media with Stefan blowing and multiple slip effects. *Comput. Math. Appl.* **2016**, *72*, 2562–2581.
22. Tausif, S.M.; Das, K.; Kundu, P.K. Multiple slip effects on bioconvection of NF flow containing gyrotactic microorganisms and nanoparticles. *J. Mol. Liq.* **2016**, *220*, 518–526.
23. Aldabesh, A.; Khan, S.U.; Habib, D.; Waqas, H.; Iskander, T.M.; Khan, I. Unsteady transient slip flow of Williamson NF containing gyrotactic microorganism and activation energy. *Alex. Eng. J.* **2020**, *59*, 4315–4328. [CrossRef]
24. Haq, F.; Kadry, S.; Chu, Y.M.; Khan, M.; Ijaz, K.M. Modeling and theoretical analysis of gyrotactic microorganisms in radiated nanomaterial Williamson fluid with activation energy. *J. Mater. Res. Technol.* **2020**, *9*, 10468–10477. [CrossRef]
25. Hussain, A.; Malik, M.Y. MHD NF flow over stretching axisymmetric cylinder with convective boundary conditions and Nield conditions in the presence of gyrotactic swimming microorganism: A biomathematical model. *Int. Commun. Heat Mass Transfer* **2021**, *126*, 105425–105436. [CrossRef]
26. Shi, Q.H.; Hamid, A.; Khan, M.I. Numerical study of bio-convection flow of magneto-cross NF containing gyrotactic microorganisms with activation energy. *Sci. Rep.* **2021**, *11*, 16030–16045. [CrossRef]
27. Yusuf, T.A.; Mabood, F.; Prasannakumara, B.C.; Sarris, I.E. Magneto-bioconvection flow of Williamson NF over an inclined plate with gyrotactic microorganisms and entropy generation. *Fluids* **2021**, *6*, 109. [CrossRef]
28. Reddy, P.S. Impact of chemical reaction and double stratification on heat and mass transfer characteristics of NF flow over porous stretching sheet with thermal radiation. *Int. J. Ambient Energy* **2020**, *43*, 1626–1636. [CrossRef]
29. Sreedevi, P.; Reddy, P.S. Williamson hybrid NF flow over swirling axisymmetric cylinder with Cattaneo-Christov heat flux and gyrotactic microorganism. *Waves Random Complex Medium* **2021**, *147*, 1968537–1968539.
30. Elbashbeshy, E.M.A.; Hamada, G.; Asker, K.M. Flow and heat transfer over a stretching surface. *Therm. Sci.* **2019**, *23*, 3105–3116. [CrossRef]

31. Shoaib, M.; Raja, M.A.Z.; Sabir, M.T.; Islam, S.; Shah, Z.; Kumam, P.; Alrabaiah, H. Numerical investigation for rotating flow of MHD hybrid nanofluid with thermal radiation over a stretching sheet. *Sci. Rep.* **2020**, *10*, 18533. [CrossRef]
32. Ullah, H.; Shoaib, M.; Khan, R.A.; Nisar, K.S.; Raja, M.A.Z.; Islam, S. Soft computing paradigm for heat and mass transfer characteristics of nanofluid in magnetohydrodynamic (MHD) boundary layer over a vertical cone under the convective boundary condition. *Int. J. Model. Simul.* **2023**, 1–25. [CrossRef]
33. Uddin, I.; Ullah, I.; Zahoor Raja, M.A.; Shoaib, M.; Islam, S. Thermal performance of chemically reactive transient thin film flow of Maxwell nanofluid with activation energy: Novel computational intelligent networks. *Waves Random Complex Media* **2022**, 1–22. [CrossRef]
34. Shoaib, M.; Ullah, I.; Raja, M.A.Z.; Farhat, I.; Sabir, M.T. Flow of magnetized nanomaterials through movable parallel plates with Lorentz forces: An intelligent computing application. *Waves Random Complex Media* **2022**, 1–22. [CrossRef]
35. Sabir, Z.; Ayub, A.; Guirao, J.L.; Bhatti, S.; Shah, S.Z.H. The effects of activation energy and thermophoretic diffusion of nanoparticles on steady micropolar fluid along with Brownian motion. *Adv. Mater. Sci. Eng.* **2020**, *2020*, 2010568. [CrossRef]
36. Bilal, M.; Saeed, A.; Gul, T.; Kumam, W.; Mukhtar, S.; Kumam, P. Parametric simulation of micropolar fluid with thermal radiation across a porous stretching surface. *Sci. Rep.* **2022**, *12*, 2542. [CrossRef] [PubMed]
37. Ali, I.; Gul, T.; Khan, A. Unsteady Hydromagnetic Flow over an Inclined Rotating Disk through Neural Networking Approach. *Mathematics* **2023**, *11*, 1893. [CrossRef]
38. Usman, M.; Gul, T.; Khan, A.; Alsubie, A.; Ullah, M.Z. Electromagnetic couple stress film flow of hybrid nanofluid over an unsteady rotating disc. *Int. Commun. Heat Mass Transf.* **2021**, *127*, 105562. [CrossRef]
39. Ullah, A.Z.; Guo, X.; Gul, T.; Ali, I.; Saeed, A.; Galal, A.M. Thin film flow of the ternary hybrid nanofluid over a rotating disk under the influence of magnetic field due to nonlinear convection. *J. Magn. Magn. Mater.* **2023**, *573*, 170673. [CrossRef]
40. Ali, A.; Khatoon, R.; Ashraf, M.; Awais, M. Cattaneo–Christov heat flux on MHD flow of hybrid nanofluid across stretched axisymmetric cylinder with radiations and Joule heating effects. *Waves Random Complex Media* **2022**, 1–18. [CrossRef]
41. Awwad, F.A.; Ismail, E.A.; Gul, T. Heat and Mass Transfer Gravity Driven Fluid Flow over a Symmetrically-Vertical Plane through Neural Networks. *Symmetry* **2023**, *15*, 1288. [CrossRef]
42. Sowmya, G.; Varun Kumar, R.S.; Alsulami, M.D.; Prasannakumara, B.C. Thermal stress and temperature distribution of an annular fin with variable temperature-dependent thermal properties and magnetic field using DTM-Pade approximant. *Waves Random Complex Media* **2022**, 1–29. [CrossRef]
43. Krishnamurthy, M.; Reddy, R.G.; Alsulami, M.D.; Prasannakumara, B.C. Numerical investigation on the effect of electrical force and periodic force on neutrally buoyant spherical particles in a Newtonian fluid at low Reynolds numbers. *Int. Commun. Heat Mass Transf.* **2022**, *135*, 106157. [CrossRef]